Flow, waves and water exchange in the Suur Strait, Gulf of Riga, in 2008*

OCEANOLOGIA, 53 (1), 2011.
pp. 35–56.

© *2011, by Institute of Oceanology PAS.*

KEYWORDS
Flow
Water exchange
Waves
Modelling
Shear velocity
Strait
Baltic Sea

Urmas Raudsepp⋆
Jaan Laanemets
Getli Haran
Victor Alari
Juss Pavelson
Tarmo Kõuts

Marine Systems Institute,
Tallinn University of Technology,
12618 Akadeemia 15a, Tallinn, Estonia;

e-mail: raudsepp@phys.sea.ee

⋆corresponding author

Received 23 June 2010, revised 26 August 2010, accepted 23 November 2010.

Abstract

Wind, flow and wave measurements were performed in November–December in 2008 in the relatively narrow and shallow Suur Strait connecting the waters of the Väinameri and the Gulf of Riga. During the measurement period wind conditions were extremely variable, including a severe storm on 23 November. The flow speed along the strait varied between ± 0.2 m s^{-1}, except for the 0.4 m s^{-1} that occurred after the storm as a result of the sea level gradient. The mean and maximum

* The work was partially supported by the Estonian Science Foundation (Grant 7283) and by the Estonian Road Administration project Perspective Development Plan for the Transportation of Passengers and Cargo across the Suur Strait and Strategic Environmental Impact Assessment.

The complete text of the paper is available at http://www.iopan.gda.pl/oceanologia/

significant wave heights were 0.53 m and 1.6 m respectively. Because of their longer fetch, southerly winds generated higher waves in the strait than winds from the north. All wave events caused by the stronger southerly winds induced sediment resuspension, whereas the current-induced shear velocity slightly exceeded the critical value for resuspension only when the current speed was 0.4 m s^{-1}. A triple-nested two-dimensional high resolution (100 m in the Suur Strait) circulation model and the SWAN wave model were used to simulate water exchange in 2008 and the wave-induced shear velocity field in the Suur Strait respectively. Circulation model simulations demonstrated that water exchange was highly variable, that cumulative transport followed an evident seasonal cycle, and that there was an gross annual outflow of 23 km^3 from the Gulf of Riga. The horizontal distribution of wave-induced shear velocity during the strong southerly wind event indicated large shear velocities and substantial horizontal variability. The shear velocities were less than the critical value for resuspension in the deep area of the Suur Strait.

1. Introduction

Shallow and narrow straits play an important role in water and material exchange between the open sea and coastal water basins, lagoons and bays. In shallow straits wind forcing generates current and sea level differences between sub-basins, which in turn influences currents. Wind-generated waves can also contribute to the flow in shallow straits. High resolution model studies of the transport of sedimentary material have shown that despite strong currents, wave action dominates the forcing of sediment transport in shallow sea areas (Seifert et al. 2009).

The Suur Strait is a relatively narrow and shallow strait connecting the waters of the Väinameri and the Gulf of Riga. The Suur Strait is the narrowest (6 km) in the Virtsu-Kuivastu region (Figure 1). Its maximum depth is 21 m and the sill depth is about 5 m near the southern side of the Väinameri basin. Besides the Irbe Strait, the Suur Strait is an alternative gateway to the Gulf of Riga, but with a cross-section that is almost nine times smaller. The gulf (area about 140×150 km^2, volume 406 km^3 and mean depth 23 m) annually receives an average of ca 32 km^3 freshwater from rivers (mainly from the Daugava).

The first current velocity measurements in the Suur Strait date back to 1908 (Mardiste 1995). In the 1990s prolonged measurement series were carried out in the Suur Strait (Suursaar et al. 1995, Suursaar et al. 1996, Suursaar et al. 1998). In the observation series of the Suur Strait, two current directions dominated: 130–160° (inflow to the Gulf of Riga) and 340–350° (outflow from the Gulf of Riga), which were in relatively good agreement with the axis of the strait. A maximum flow speed of about 1 m s^{-1} was recorded in both along-axis directions during ice-free conditions in the winter of 1994/95. In spring and summer the flow speeds were about

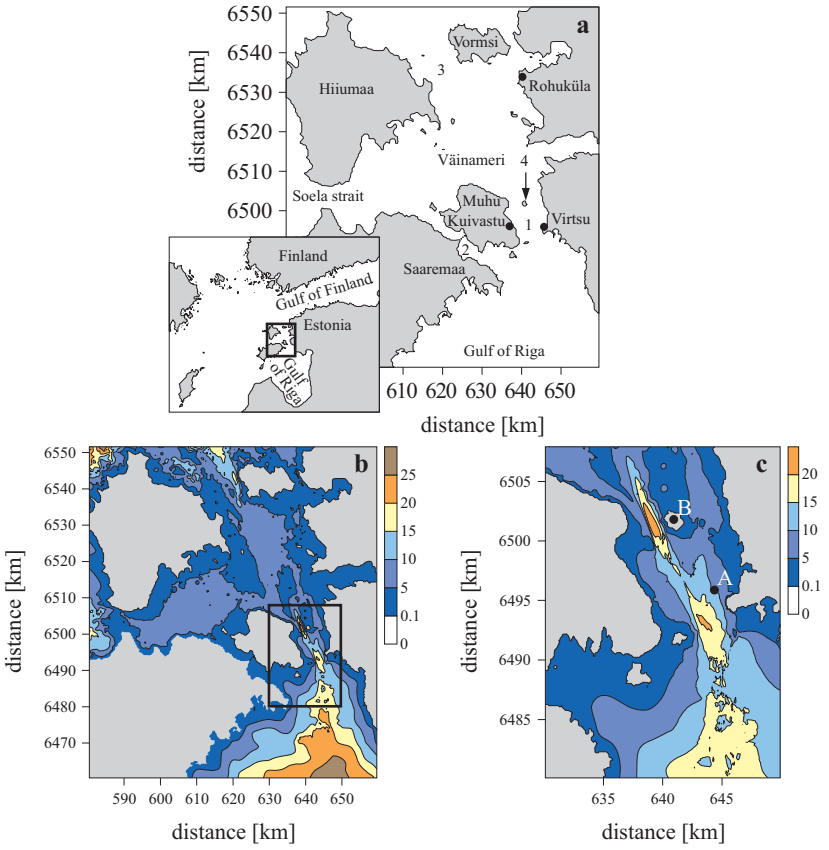

Figure 1. Study area (a). 1 – Suur Strait; 2 – Väike Strait; 3 – Hari Strait; 4 – Kessulaid. The bottom topography of the Väinameri region used in the 400 m resolution wave model (b). The black rectangle represents the borders of the 100 m model. The high resolution bottom topography of the Suur Strait (c). The filled circles (A) and (B) mark the positions of the buoy station and the weather station respectively. Coordinate system UTM-34. Colour scale: depth in metres

half as fast as the winter ones without ice cover. In winter with ice cover the flow speeds were relatively small: 0.05–0.15 m s^{-1} (mean) and up to 0.35 m s^{-1} (maximum).

Water exchange through the Suur Strait has been estimated from direct current velocity measurements and from model simulations. The yearly inflow to the Gulf of Riga has been estimated at between 110 and 159 km^3, while the yearly outflow is between 133 and 201 km^3 (Suursaar et al. 1996, Otsmann et al. 2001). These estimates give a gross outflow from the Gulf of Riga of between 10 and 53 km^3. On the basis of these estimates, the flow

through the Suur Strait plays an important role (up to 32%) in the water balance of the Gulf of Riga (Suursaar et al. 1996).

Surface wave measurements in the Suur Strait have not been carried out, although the role of waves can be important in forcing currents, and more likely, in resuspending bottom sediments. Mulligan et al. (2008) have shown the importance of wave-induced currents in the overall circulation in the small and shallow Lüneburg Bay during the passage of a hurricane.

There is still no evidence for the effect waves may have on resuspension and what the contribution of wave-induced currents in the overall water exchange in the Suur Strait could be. The objectives of this paper were (1) to simulate flow velocity and surface wave fields in the Suur Strait and to validate these with in situ observations; (2) using simulation results, to estimate the proportion of surface waves in the flow field and water exchange through the Suur Strait; and (3) using observation data and model simulations, to estimate wave-induced and current-induced shear velocities.

This paper is structured as follows. In section 2, the field data, circulation model and wave model are briefly described, and the wave and current shear velocities are calculated. In section 3, the model results are presented, discussed and compared with the measurements. The conclusions are drawn in section 4.

2. Data and methodology

2.1. Field measurements

Current velocity and wave measurements in the Suur Strait were performed in November–December 2008. A buoy station equipped with a Sensordata current meter SD-6000 and a pressure sensor was deployed on 13 November near Virtsu (58°34.95′N; 23°29.30′E, Figure 1c). The water depth at the location of the buoy station was 9 m. The current meter was at a depth of 3.5 m and the wave gauge at 2.5 m. The current speed and direction recording interval was 5 min, that of the wave gauge 0.25 s. Current measurements lasted until 4 December and wave measurements until 6 December. The method for reconstructing surface elevation spectra from sub-surface pressure recordings is described in detail by Alari et al. (2008).

Wind speed and direction were recorded with the Väisälä Weather Transmitter WXT520 installed at a height of 30 m at the Kessulaid weather station (Figure 1c). It recorded wind data at 5 min intervals from 21 November to 13 December. We used a height correction factor of 0.91 to reduce the recorded wind speed to the reference height of 10 m (Launiainen & Laurila 1984).

2.2. Description of the circulation model

We used a two-dimensional circulation model based on the hydrodynamic equations for a shallow sea. The model had been applied earlier to different regions of the Estonian coastal sea (Sipelgas et al. 2006). The model consists of vertically integrated motion equations

$$\frac{\partial u}{\partial t} + u\frac{\partial u}{\partial x} + v\frac{\partial u}{\partial y} - fv = -g\frac{\partial \eta}{\partial x} + \frac{F_w^x}{h} - \frac{F_b^x}{h} + \frac{F_{\text{wave}}^x}{h} + G^x, \tag{1}$$

$$\frac{\partial v}{\partial t} + u\frac{\partial v}{\partial x} + v\frac{\partial v}{\partial y} + fu = -g\frac{\partial \eta}{\partial y} + \frac{F_w^y}{h} - \frac{F_b^y}{h} + \frac{F_{\text{wave}}^y}{h} + G^y$$

and a continuity equation

$$\frac{\partial \eta}{\partial t} + \frac{\partial uh}{\partial x} + \frac{\partial vh}{\partial y} = 0, \tag{2}$$

where (u, v) are the vertically averaged velocities in the water column in the Cartesian coordinates, (F_w^x, F_w^y) are the kinematic wind stresses, (F_b^x, F_b^y) are the bottom friction stresses, $(F_{\text{wave}}^x, F_{\text{wave}}^y)$ are the wave-induced forces, (G^x, G^y) are the horizontal turbulent viscosities in the (x, y) directions, f is the Coriolis parameter, g is the acceleration due to gravity, η is the sea surface elevation (deviation from the equilibrium depth) and $h(x, y)$ is the depth.

In order to take into account the wave-induced currents, a wave-induced force per unit surface area is added to the kinematic wind stress in both the x and the y directions. The wave-induced force per unit surface area [N m^{-2}] is calculated as the gradient of the radiation stresses (SWAN 2008).

The friction at the bottom is calculated using the quadratic relationship from the flow speed

$$F_b^x = C_D|\overrightarrow{u}|u, \;\; F_b^y = C_D|\overrightarrow{u}|v, \tag{3}$$

where $C_D(= 2.5 \times 10^{-3})$ is the bottom friction coefficient, and $\overrightarrow{u}$ is the current velocity. The bottom friction coefficient is taken to be constant, since reliable data on sea bottom irregularities are lacking. The wave-induced force per unit surface area is the gradient of radiation stresses. It reads:

$$F_{\text{wave}}^x = \frac{1}{\rho_0}\left(-\frac{\partial S_{xx}}{\partial x} - \frac{\partial S_{xy}}{\partial y}\right), \;\; F_{\text{wave}}^y = \frac{1}{\rho_0}\left(-\frac{\partial S_{yx}}{\partial x} - \frac{\partial S_{yy}}{\partial y}\right), \tag{4}$$

where ρ_0 is the reference density and S is the radiation stress tensor as given by

$$S_{xx} = \rho_0 g \int n\cos^2\theta + n\,\frac{1}{2}\,Ed\sigma d\theta, \tag{5}$$

$$S_{xy} = S_{yx} = \rho_0 g \int n\sin\theta\cos\theta Ed\sigma d\theta,$$

$$S_{yy} = \rho_0 g \int \left[n\sin^2\theta + n - \frac{1}{2}\right] Ed\sigma d\theta,$$

where n is the ratio of the group velocity to the phase velocity. $E(\sigma,\theta)$ denotes the two-dimensional wave spectrum in frequency and directional space respectively.

The terms of horizontal turbulence are calculated using the constant eddy viscosity coefficient A_H:

$$G^x = A_H\left(\frac{\partial^2 u}{\partial x^2} + \frac{\partial^2 u}{\partial y^2}\right),\ G^y = A_H\left(\frac{\partial^2 v}{\partial x^2} + \frac{\partial^2 v}{\partial y^2}\right). \tag{6}$$

The eddy viscosity coefficient for all grids is 50 $\mathrm{m^2\ s^{-1}}$.

The kinematic wind stress components are calculated as:

$$F_x^w = \frac{\tau_x^w}{\rho_0} = \frac{\rho_a}{\rho_0} c_d u_w |\overrightarrow{u}_w|, \tag{7}$$

$$F_y^w = \frac{\tau_y^w}{\rho_0} = \frac{\rho_a}{\rho_0} c_d v_w |\overrightarrow{u}_w|,$$

where $\overrightarrow{u}_w$ is the wind velocity vector, u_w and v_w are wind components, τ_x^w and τ_y^w are wind stress components, $c_d (= 1.3 \times 10^{-3})$ is the drag coefficient, and ρ_a is the air density.

Thus, the numerical model takes into account bottom topography, the Earth's rotation, friction at the sea bottom and horizontal eddy viscosity. Temperature and salinity fields are not calculated in the model. Consequently, the baroclinic component of currents is not taken into account; in the Väinameri region this is of minor importance compared to wind forcing and sea level changes (Otsmann et al. 2001).

The model did not include the river runoff into the Gulf of Riga because of its minor role in the water exchange through the Suur Strait. According to previous modelling studies, the river inflow affects mainly the flows in the Irbe Strait because the Suur Strait has a smaller cross-section and a higher resistance (Otsmann et al. 1997, Otsmann et al. 2001, Suursaar et al. 2002: Figure 3f).

A triple-nested circulation model was used for the simulation of currents and water exchange in the Suur Strait. The coarse grid model covered the whole Baltic Sea with a spatially constant grid size of 2x2 km. Digital

topography was taken from Seifert et al. (2001). No open boundary conditions were implemented for this grid. The model for the Väinameri region had a grid size of 400x400 m (Figure 1b), whereas the boundary conditions for water transport were obtained from the whole Baltic Sea model. The high resolution model for the Suur Strait area had a grid step of 100x100 m (Figure 1c), and boundary conditions were obtained from the Väinameri model. One-way grid nesting was used for both model domains. For the Väinameri and the Suur Strait models, transport was used as a boundary condition. In the Väinameri and Suur Strait models, bottom topography was based on marine charts, the data being obtained from hydrographical surveys by the Estonian Maritime Administration.

Hydrodynamic model forcing was obtained from the atmospheric model HIRLAM (High Resolution Limited Area Model) version of the Swedish Meteorological and Hydrological Institute in the form used for the forcing of the HIROMB (High Resolution Operational Model of the Baltic Sea) model. Wind velocity components were interpolated to all three model grids. The HIRLAM winds were compared with the measured local wind data at the Kessulaid station. The wind velocity interpolated from the HIRLAM data was smaller than that of the wind measurements at Kessulaid by a factor of 1.4 and were therefore multiplied by this factor.

2.3. Description of the wave model

The SWAN wave model was implemented to describe wave conditions in the Väinameri. The SWAN model is a third-generation, phase-averaged spectral wave model developed at the Delft University of Technology (Booij 1999). In SWAN, the waves are described with the two-dimensional wave action density spectrum, whereas the evolution of the action density N is governed by the time-dependent wave action balance equation, which reads:

$$\frac{\partial N}{\partial t} + \nabla \times \left[\left(\overrightarrow{c}_g + \overrightarrow{U}\right)N\right] + \frac{\partial c_\sigma N}{\partial \sigma} + \frac{\partial c_\theta N}{\partial \theta} = \frac{S_{\mathrm{tot}}}{\sigma}. \tag{8}$$

The first term represents the local rate of change of action density; the second term denotes the propagation of wave energy in two-dimensional geographical space, with $\overrightarrow{c}_g$ being the group velocity and $\overrightarrow{U}$ the ambient current. The third term represents the effect of shifting of the radian frequency due to variations in depth and mean currents. The fourth term represents the depth-induced and current-induced refraction. The quantities c_σ and c_θ are the propagation velocities in spectral space (σ, θ), with σ and θ representing the radian frequency and propagation direction respectively. The right-hand side contains the source term S_{tot} representing all the

physical processes that generate, dissipate or redistribute wave energy. In shallow water, six processes contribute to S_{tot}:

$$S_{\mathrm{tot}} = S_{\mathrm{wind}} + S_{nl3} + S_{nl4} + S_{wc} + S_{\mathrm{bot}} + S_{db}. \tag{9}$$

These terms denote the energy input by wind (S_{wind}), the nonlinear transfer of wave energy through three-wave (S_{nl3}) and four-wave interactions (S_{nl4}), and the dissipation of waves due to whitecapping (S_{wc}), bottom friction (S_{bot}) and depth-induced wave breaking (S_{db}) respectively. Extensive details on the formulations of these processes can be found, for example, in Komen et al. (1994).

For the present calculations with SWAN, the same bottom topography and meteorological forcing was used as in the circulation model. The third-generation model was used with respect to wind-input, quadruplet interactions and whitecapping. Triads, bottom friction and depth-induced breaking were also activated. For wind-input and whitecapping dissipation, the formulation by Van der Westhuysen et al. (2007) was used; in the case of wind-input, only the exponential growth term was activated. The quadruplet interaction was approximated using the Discrete Interaction Approximation (DIA). Wave breaking is governed by the ratio of the maximum individual wave height to the depth and was set at 0.73. A semi-empirical expression for bottom friction (see Holthuijsen 2007) was also activated.

2.4. Wave and current shear velocities

Sediment resuspension by waves commences when fluid flow forces, such as shear stress (or shear velocity), exceed the resisting forces such as gravity and bottom friction (Van Rijn 2007). Water depth, significant wave height and peak period dictate wave-generated shear velocities acting on deposited material. In order to calculate the wave-induced shear velocity at the bottom, the near-bottom excursion amplitude and orbital velocity were calculated using the respective formulas by Kuhrts et al. (2004):

$$A_b = \frac{H_s}{2\sinh\left(\dfrac{2\pi h}{\lambda}\right)}, \tag{10}$$

$$U_b = 2\pi\frac{A_b}{T_p},$$

where H_s is the significant wave height, λ is the wavelength (corresponding to the peak wave period), T_p is the peak wave period and h is the water

depth. The shear velocity also depends on the friction coefficient f_w, which is calculated as follows:

$$f_w = \left\{ \begin{array}{l} 0.3, \ \frac{A_b}{2.5d} < 1.57 \\ \exp\left(5.5\left(\frac{A_b}{2.5d}\right)^{-0.2}\right) - 6.3 \end{array} \right\}, \tag{11}$$

where d is the diameter of the particulate matter. The shear velocity therefore takes the following form:

$$u_s = U_b\sqrt{0.5 f_w}. \tag{12}$$

The current induced shear velocity was also calculated according to Kuhrts et al. (2004).

3. Results and discussion

3.1. Wind conditions

Moderate southerly winds dominated during the measurement period (Figures 2a and b), and the mean wind speed was 7.0 ± 3.5 m s^{-1}. Long-term analyses of winds at Vilsandi meteorological station showed an angular

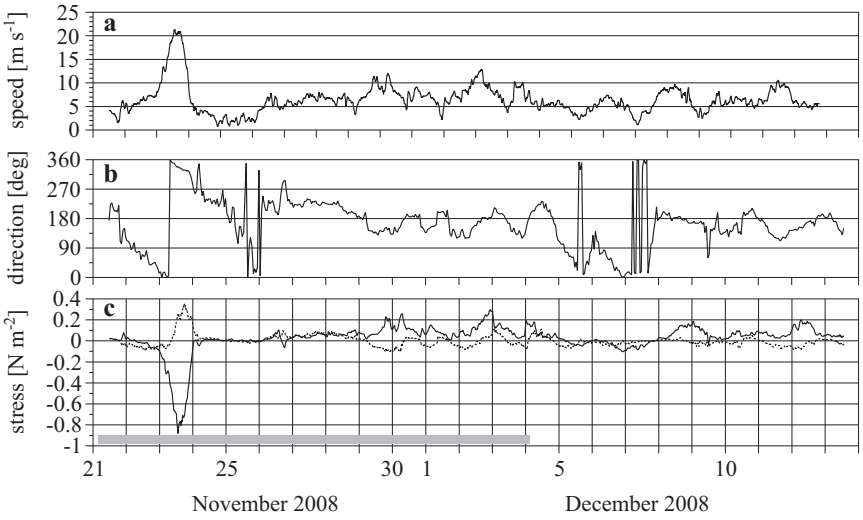

Figure 2. Wind speed (a), direction (b) and along-strait wind stress component (solid curve) and cross-strait wind stress component (dotted curve) calculated from wind data (c). The x-axis is positive eastwards, the y-axis is positive northwards. The shaded rectangle on the x-axis shows the period of current measurements. The data are smoothed with a 1 h running mean

distribution of directions with two peaks (Soomere & Keevallik 2003): the dominant wind direction is SW, and secondarily N or NNW, which means that our measurements represent the prevailing winds in the area. A strong storm passed through the study area on 23 November, when the maximum NNW wind speed was 23 m s^{-1} and up to 30 m s^{-1} during gusts.

The along- and cross-strait components of the wind stress were calculated in the Suur Strait (eq. (7)). Five wind impulses with an absolute along-strait wind stress component ≥ 0.2 N m^{-2} could be identified, whereas during the storm of 23 November the maximum along-strait wind stress values were ca -0.9 N m^{-2} (Figure 2c).

3.2. Flow in the strait

The cross-strait flow velocity component u and the along-strait flow velocity component v were calculated from current meter data (Figure 3). The along-strait velocity component describes water exchange in the strait, whereas the inflow to the strait means northward motion, i.e. positive v values.

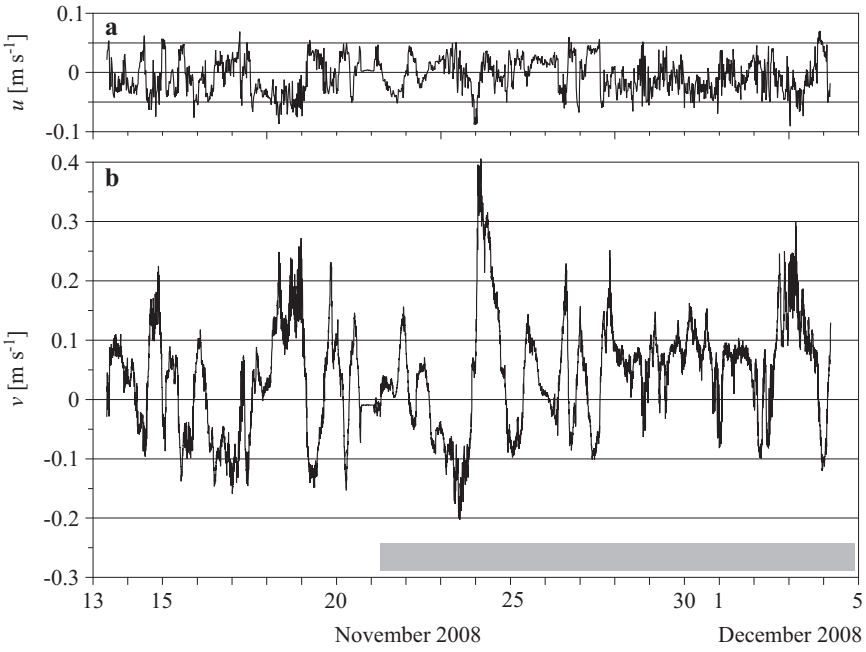

Figure 3. The cross-strait flow velocity component u (a) and the along-strait velocity component v (b) calculated from the measured current data in the Suur Strait. The shaded rectangle on the x-axis shows the period of wind measurements

During the severe storm on 23 November the southward flow speed was up to 0.2 m s^{-1}, the flow being from the Väinameri to the Gulf of Riga (Figure 3b). The highest along-strait flow speeds were measured after the passage of the storm and were up to 0.4 m s^{-1} (directed northwards). The somewhat lower flow speed than previously reported by Otsmann et al. (2001) was due to the closer location of our buoy station to the coast. Cross-strait flow speeds were small and varied mainly between −0.05 and +0.05 m s^{-1} (Figure 3a).

The correlation between the along-strait wind stress and the flow speed was low (r = 0.53), indicating the important role of the along-strait sea level gradient in flow generation. From the sea level changes measured at the Virtsu and Rohuküla stations (Figure 1a), it can be seen that on the morning of 23 November, the sea level difference between Virtsu and Rohuküla started to increase rapidly and was about 0.4 m on the morning of 24 November (Figure 4). This is most likely the reason why during the gale the southward flow speeds were relatively small and during the rapid decrease in wind speed on 24 November, a strong northward flow was forced by the along-strait sea level gradient.

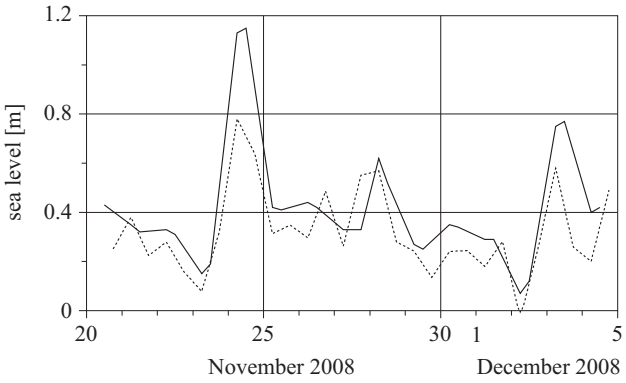

Figure 4. The course of sea level at Virtsu (solid curve) and Rohuküla (dotted curve) stations. (Data from the Estonian Meteorological and Hydrological Institute)

The flow in the Suur Strait was also characterized by well-expressed oscillations with different periods (Figure 3b). Otsmann et al. (2001) found from the spectral analysis of current measurements that the duration of the only significant oscillation period in the Suur Strait was 12.43 h, which is close to the M_2 (lunar semi-diurnal) tidal period (12.42 h). They also modelled the flow in the straits as the superposition of two Helmholtz oscillators with resonance periods of about 13 and 24 h. These

oscillations appeared as a response of the system both to rapid changes in the wind forcing and to the sea level changes in the boundaries of the study area.

3.3. Wave characteristics

The mean significant wave height during the measurements was 0.53 m and the maximum significant wave height was 1.6 m (Figure 5a). Six events when the significant wave height grew to over 1 m were observed during the measurement period. The mean peak period during the measurements was 4.5 s and varied between 2.3 s and 8 s (Figure 5b). The peak period grew during the larger wave events. The maximum wave height was 2.5 m during the measurement campaign.

The first stronger wave event occurred in the evening of 14 November, when the significant wave height reached 1.35 m and the maximum peak period was about 7 s. The wind was blowing from the south at a speed of 12 m s^{-1} (HIRLAM data). The fetch length of southerly waves was about 170 km. The strongest wave event occurred on 18 November, during which the significant wave height reached 1.6 m and the peak wave period was

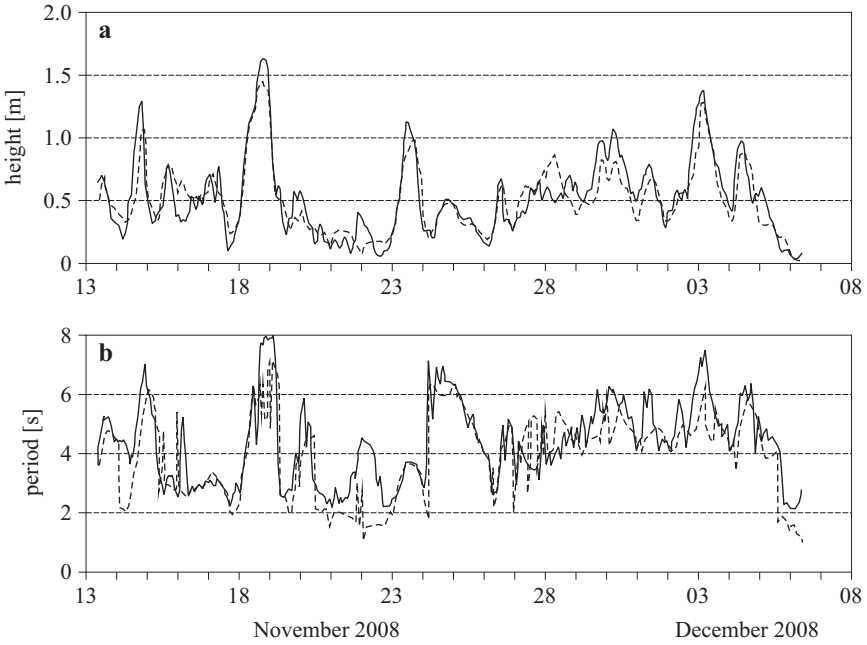

Figure 5. Measured (solid line) and modelled (dashed line) wave parameters: the significant wave height (a) and the peak period (b). The horizontal axis represents dates in November–December

8 s. This event was the result of southerly winds blowing at speeds of up to 15 m s^{-1} (HIRLAM data).

Although the strongest wind was measured on 23 November (23 m s^{-1} from the NNW (Figures 2a and b)), it did not generate the highest waves – the significant wave height remained below 1.2 m and the peak wave period was 3.7 s. At the end of November, an SSE wind with a speed up to 11 m s^{-1} excited waves with a significant height of 1.1 m and a period of 6 s. The southerly wind of 13 m s^{-1} on the night of 3 December resulted in a significant wave height of about 1.4 m, with a peak wave period of 7 s.

On the afternoon of 24 November a swell was measured, where the significant wave height was between 0.4 and 0.5 m and the associated peak wave period was over 7 s. The speed of the wind, blowing from the SW, measured at the Kessulaid weather station was < 5 m s^{-1}. The wave spectrum during this time was shifted towards lower frequencies compared to the spectra from stormy conditions (Figure 6). At first glance, we could explain this swell as a consequence of the strong, 23 m s^{-1}, NNW wind on 23 November. But the wind dropped some 12 h (Figure 2) before the first signs of swell. Therefore, it is rather unlikely that long swells could flow into the Suur Strait from the rather shallow Väinameri area. Examining the HIRLAM wind field for this period (24 November), one could see a SW

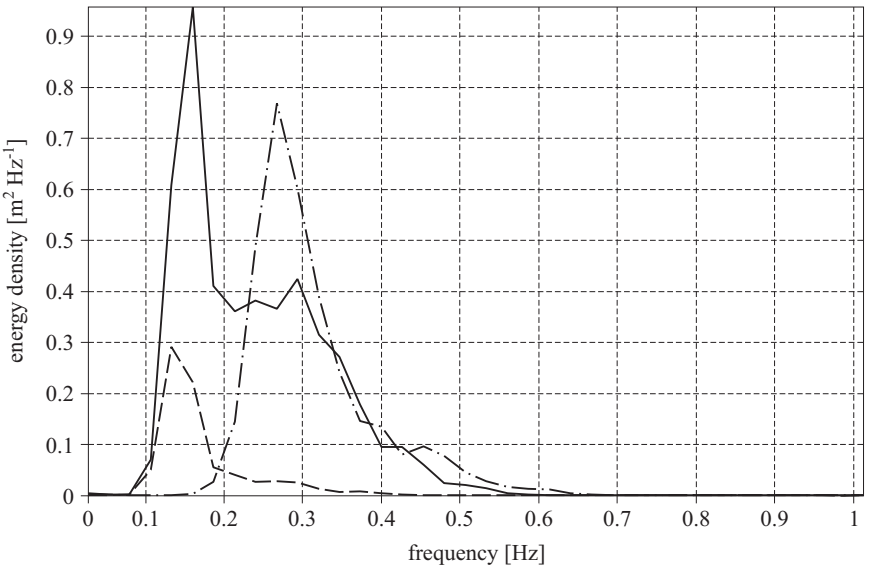

Figure 6. The wave field spectra during the observation period: a long fetch and the S wind on 14 November (solid line), a short fetch and the NNW storm wind on 23 November (dash-dot line) and the swell (dashed line)

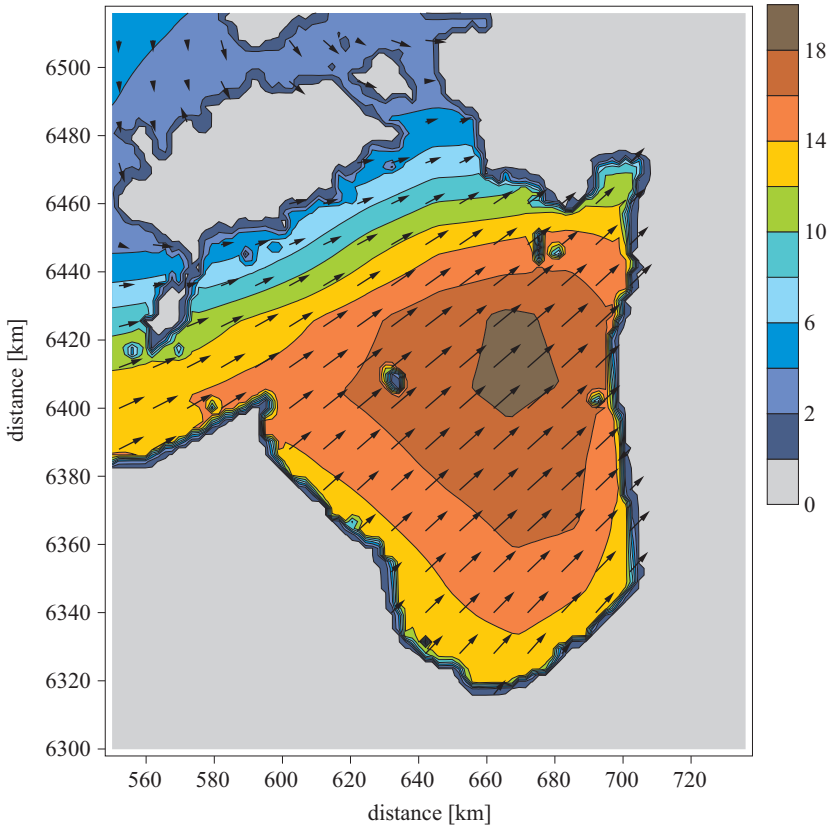

Figure 7. Wind field of HIRLAM (speed and direction) over the Gulf of Riga on 24 November at 11.00 UTC. Colour scale: wind speed in m s^{-1}

storm in the Gulf of Riga with wind speeds of up to 18 m s^{-1} (Figure 7). The wind speed decreased significantly towards the Väinameri and matched the measured value at Kessulaid. Thus, the swell at the measurement site can be explained as having been generated by the SW storm in the open Gulf of Riga.

The wave field is described by the long fetch (the S wind), the short fetch (the NNW wind) and the swell spectrum during the observation period (Figure 6). As one can see, the southerly wind on 14 November generated a rather broad spectrum, which had its maximum at 0.16 Hz and a secondary, lower peak at 0.3 Hz. The NNW wind on 23 November, 23 m s^{-1}, on the other hand, generated a spectrum where the peak frequency was 0.27 Hz. This was because the NNW winds had a shorter fetch than the southerly winds, so that its spectrum was shifted towards higher frequencies. For the swell coming from the south, the spectrum peak was located at 0.13 Hz and the tail of the spectrum contained less energy.

3.4. Shear velocity

The wave-induced and current-induced shear velocities were calculated from the measured time series of waves and currents (Figure 8). The critical shear velocity for the resuspension of grains 0.25 mm in size, which corresponds to the fine sand common to the Väinameri, is 1.4 cm s^{-1} (Kuhrts et al. 2004). All wave events when the wind was blowing from the south induced sediment resuspension, and the highest shear velocities were obtained during the strong (15 m s^{-1}) southerly wind event on 18 November. Note that the extreme northerly wind event on 23 November did not induce shear velocities larger than the critical value, but it is possible that the swell the next day led to resuspension. For the current-induced shear velocity, the critical value for resuspension was slightly exceeded only on 24 November, when current speeds of up to 0.4 m s^{-1} generated shear velocities of up to 1.5 cm s^{-1} in the bottom boundary layer. The root mean square difference between the wave- and current-induced shear velocities was 1.05 cm s^{-1}.

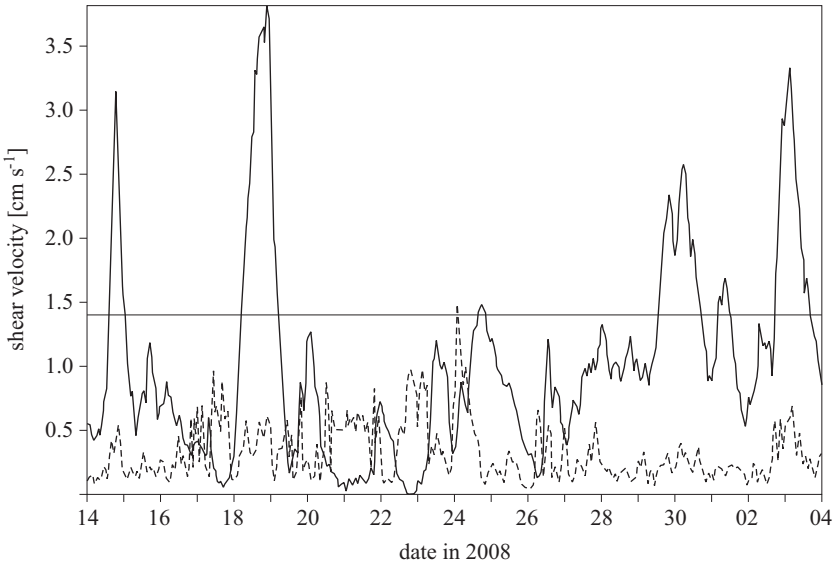

Figure 8. The wave-induced (solid line) and current-induced (dashed line) shear velocities calculated from the measured wave and current time series. The horizontal line marks the critical shear velocity (1.4 cm s^{-1}) for resuspension

The triple-nested wave model with the same bathymetry and forcing as the circulation model was used. The model results were validated using the wave measurements. The modelled and measured significant wave heights

coincided rather well – the corresponding correlation coefficient was 0.89 and the scatter index (root mean square difference between the simulated and measured significant wave height divided by the mean measured significant wave height) was 0.28. The correlation coefficient was 0.76 and the scatter index was 0.24 for peak periods.

The horizontal distribution of wave-induced shear velocities at the peak of the strong (15 m s^{-1}) southerly wind event showed great variability (Figure 9). Shear velocities were the highest, exceeding 6 cm s^{-1}, in the

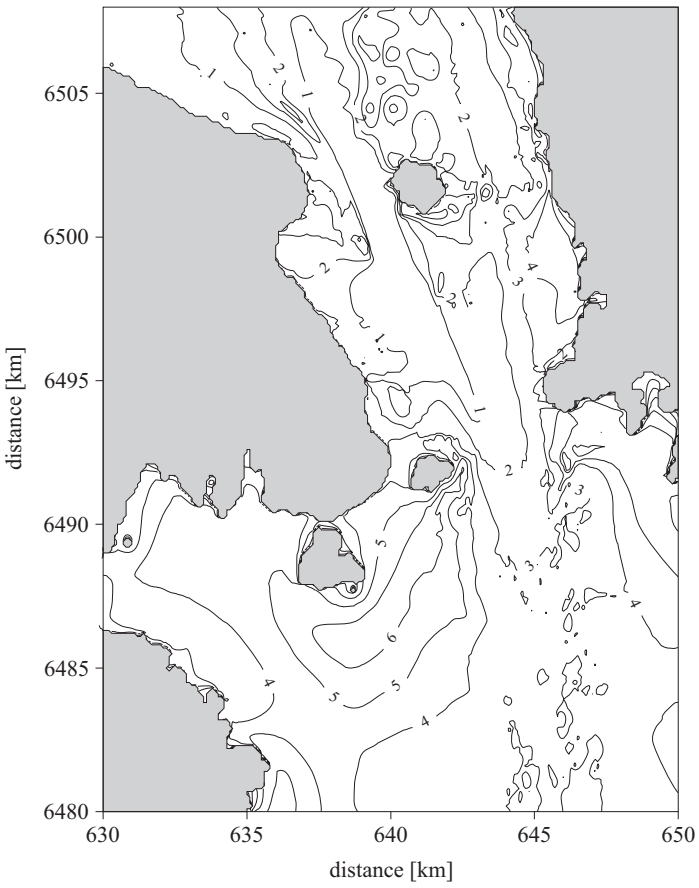

Figure 9. The map of wave-induced shear velocities at the peak of the strong southerly wind event on 18 November

southern part of the Suur Strait and were less than the critical value for resuspension in its deepest area. Thus, wave-induced shear velocities were generally related to the bottom topography of the strait.

3.5. Water exchange

The flow velocity measurements in the Suur Strait in November–December were used for the validation of the circulation models (100 m and 400 m grid step). Only the validation of the high resolution 2D circulation model with the 100 m grid step is presented because the model with the 400 m grid step gave approximately the same result. Since the models do not contain semidiurnal tidal currents, the measured flow velocity data series were smoothed with a 12 h moving average. It can be seen in Figure 10 that the rapid change in the wind field on 23 November (Figure 2) with the consequent sea level change (Figure 4) caused remarkable changes in the flow regime. The high-speed flow reversed within a short space of time. The coincidence of the measured and simulated along-strait flow speed was high – the correlation coefficient was 0.88. A certain difference can be seen in the case of higher flow speeds.

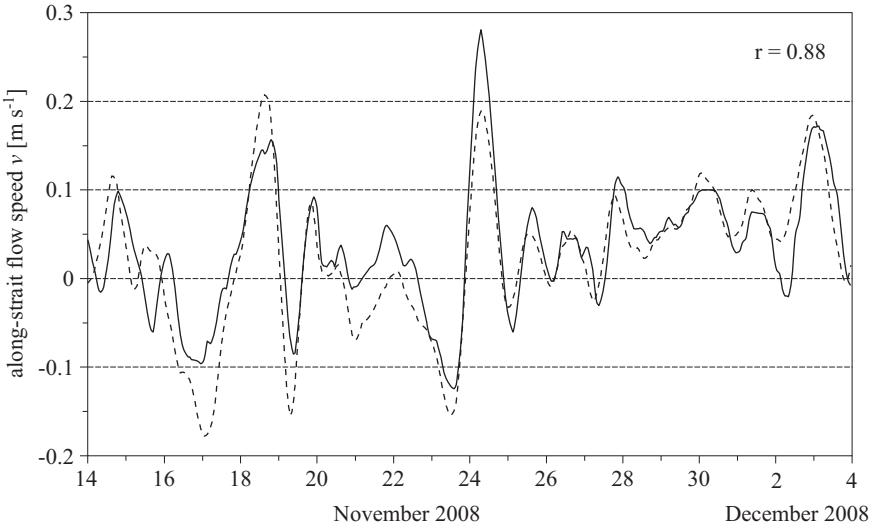

Figure 10. A comparison of simulated and measured along-strait flow speed v in the Suur Strait. Solid curve – measured flow speed, dashed curve – simulated flow speed. The model grid step is 100 m. The measured along-strait flow component v was smoothed with a 12 h running mean

Re-calculations with the circulation model were performed for November by taking into account wave stress as forcing additional to the wind. The wave stress was obtained from wave model simulations. The r.m.s. difference of the simulated along-strait flow component v with and without wave stress was 0.01 m s^{-1} over the Suur Strait model area. The estimate

was found for 19 November when the significant wave height was the highest (Figure 5a).

Wind-induced currents were much stronger in the strait area, reaching values of up to 60 cm s^{-1} (Figure 11), when wave-induced currents were negligible. However, wave-induced currents were essential in the flow field near the south-eastern tip of Muhu Island. The influence of wave stress on water exchange in the Suur Strait is insignificant. Wave-induced currents should be considered when modelling sediment transport in a shallow sea in the case of a long fetch.

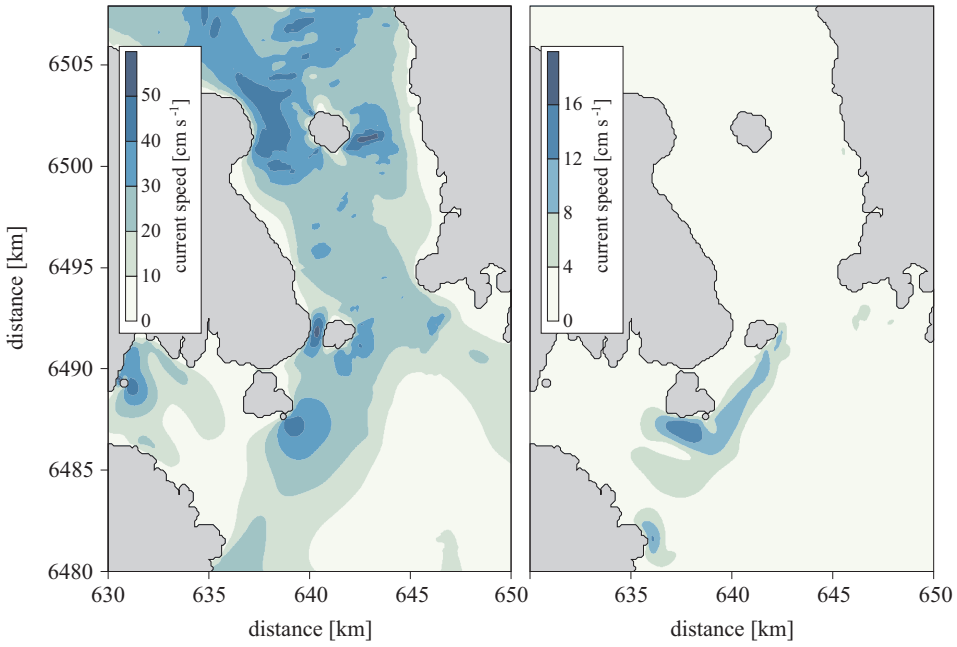

Figure 11. Maps of wind induced current speed (left) and wave induced current speed (right) in the Suur Strait at 23:00 UTC on 19 November 2008

The simulations with a validated high resolution circulation model were performed for the whole of 2008. Satellite imagery (Envisat, MERIS, ASAR) showed that the Väinameri region was practically ice free in 2008. The along-strait flow speed and direction were highly variable throughout the year (Figure 12), but water exchange was evidently seasonally variable (Figure 13). Northward flows were dominant from January until the middle of February, resulting in a 15 km^3 water transport from the Gulf of Riga to the Väinameri.

From mid-February until late April, the cumulative water exchange through the Suur Strait was small, although the instantaneous velocities were not. From May till mid-June outflow from the Väinameri to the Gulf of Riga was dominant, the corresponding cumulative water exchange being 10 km^3. From May to July the currents were less variable than during the rest of the year. During the summer months (June, July, August) the periods of outflow from the Gulf of Riga alternated with inflow.

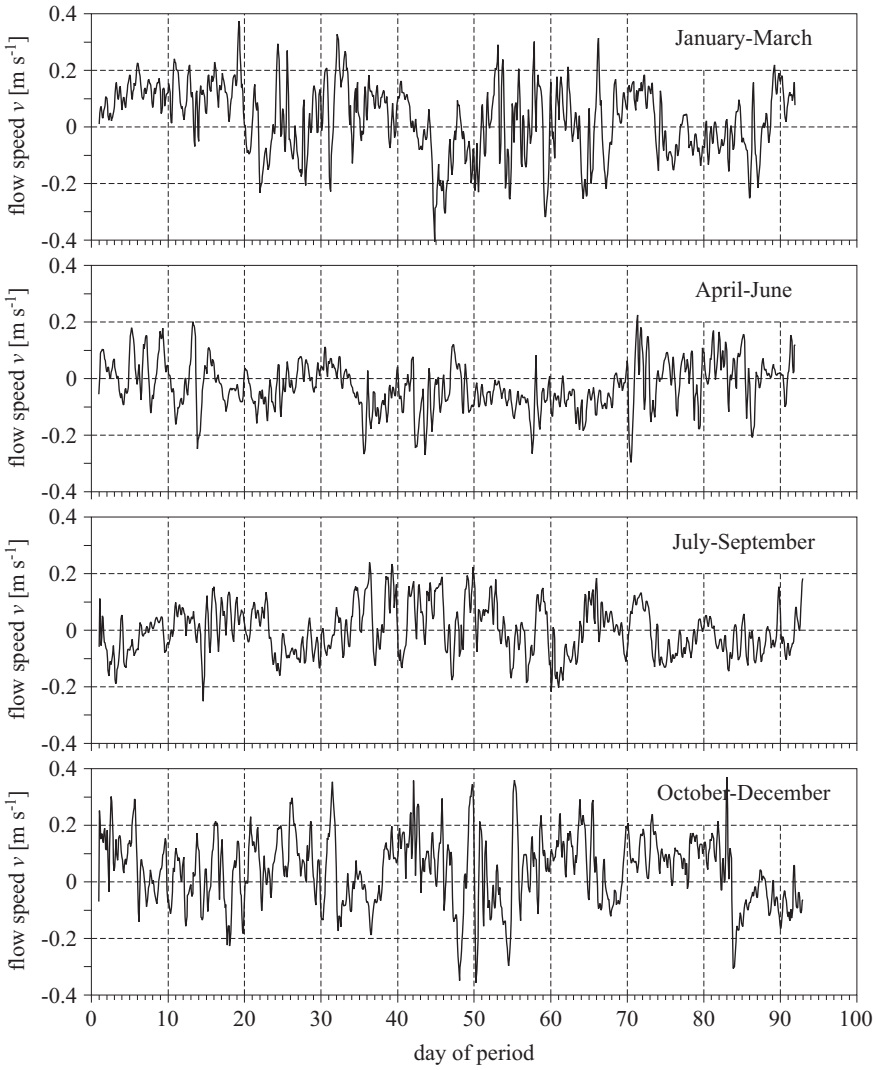

Figure 12. The simulated along-strait flow speed v at the centre of the Virtsu-Kuivastu transect during 2008

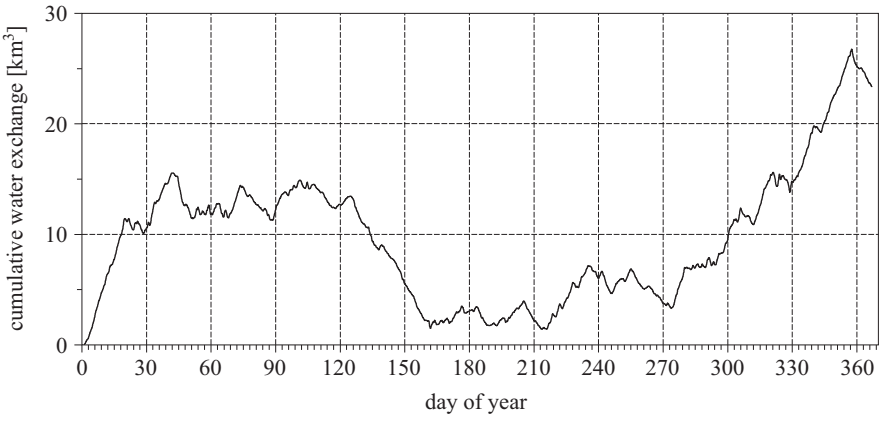

Figure 13. Cumulative water exchange through the Virtsu-Kuivastu cross-section during 2008

From October until the end of December there was a gross outflow from the Gulf of Riga to the Väinameri: the corresponding cumulative water exchange was approximately 20 km^3. The annual water exchange was about 23 km^3 from the Gulf of Riga to the Väinameri. To conclude, both the flow speed and the water exchange are characterized by considerable variability.

A dominant outflow from the Gulf of Riga to the Väinameri from late autumn to early spring is characteristic of mild winters (Otsmann et al. 2001). For instance, the winter of 1994/1995 was stormy and ice free, which resulted in a strong outflow into the Suur Strait. October–December 1996 was also windy, resulting in a persistent outflow. In contrast, the winter of 1995/1996 was cold (ice cover in the Suur Strait) and the dominant winds blew from the north. Under these conditions a weak inflow to the Gulf of Riga through the Suur Strait was observed.

4. Conclusions

1. Field measurements showed a certain asymmetry between along-strait wind forcing, flow speed and significant wave height. Because of the longer fetch of southerly waves, the highest significant wave heights (maximum 1.6 m) were observed during southerly wind events.
2. Numerical simulations with added wave stress as forcing demonstrated the minimal influence of wave-induced currents on flow speed and water exchange in the Suur Strait; nevertheless, wave-induced currents should be taken into consideration when modelling nearshore hydrodynamics.

3. Current-induced shear velocities were below the critical value for resuspension, whereas wave-induced shear velocities considerably exceeded it in cases of stronger southerly wind forcing. In general, wave-induced shear velocities were larger in the shallower areas but less than the critical value in the deep waters of the Suur Strait. Hence, the coupled wave-circulation model should be used to estimate sediment resuspension and transport in the area.
4. The simulations for the whole of 2008 showed a clear seasonal cycle with respect to cumulative transport, outflow from the Gulf of Riga during autumn and early winter, and inflow during early spring. There was an gross annual outflow of 23 km^3 from the Gulf of Riga to the Väinameri.

Further studies are needed to quantify material transport through the Suur Strait focusing on the cycling of material between sediments and water.

Acknowledgements

We thank the anonymous referees for their valuable comments on the manuscript.

References

Alari V., Raudsepp U., Kõuts T., 2008, *Wind wave measurements and modelling in Küdema Bay, Estonian Archipelago Sea*, J. Marine Syst., 74 (Suppl. 1), S30–S40.

Booij N., Ris R. C., Holthuijsen L. H., 1999, *A third-generation wave model for coastal regions. 1. Model description and validation*, J. Geophys. Res., 104 (C4), 7649–7666.

Holthuijsen L. H., 2007, *Waves in oceanic and coastal waters*, Cambridge Univ. Press, New York, 404 pp.

Komen G. J., Cavaleri L., Donelan M., Hasselmann S., Janssen P. A. E. M., 1994, *Dynamics and modelling of ocean waves*, Cambridge Univ. Press, Cambridge, 532 pp.

Kuhrts C., Fennel W., Seifert T., 2004, *Model studies of transport of sedimentary material in the western Baltic*, J. Marine Syst., 52 (1–4), 167–190.

Launiainen J., Laurila T., 1984, *Marine wind characteristics in the northern Baltic Sea*, Finnish Mar. Res., 250, 52–86.

Mardiste H., 1995, *Eestit piirava mere hüdroloogilise uurimise ajalugu (kuni 1917 aastani)*, Teaduse ajaloo lehekülgi Eestist, XI, TA Kirjastus, Tallinn, 58–78.

Mulligan R. P., Hay A. E., Bowen A. J., 2008, *Wave-driven circulation in a coastal bay during the landfall of a hurricane*, J. Geophys. Res., 113, C05026, 1–10.

Otsmann M., Astok V., Suursaar Ü., 1997, *A model for water exchange between the Baltic Sea and the Gulf of Riga*, Nordic Hydrol., 28 (4–5), 351–364.

Otsmann M., Suursaar Ü., Kullas T., 2001, *The oscillatory nature of the flows in the system of straits and small semienclosed basins of the Baltic Sea*, Cont. Shelf Res., 21 (15), 1577–1603.

Seifert T., Fennel W., Kuhrts C., 2009, *High resolution model studies of transport of sedimentary material in the south-western Baltic*, J. Marine Syst., 75 (3–4), 382–396.

Seifert T., Kayser B., Tauber F., 2001, *Bathymetry data of the Baltic Sea*, Baltic Sea Res. Inst., Warnemünde.

Sipelgas L., Raudsepp U., Kõuts T., 2006, *Operational monitoring of suspended matter distribution using MODIS images and numerical modelling*, Adv. Space Res., 38 (10), 2182–2188.

Soomere T., Keevallik S., 2003, *Directional and extreme wind properties in the Gulf of Finland*, Proc. Estonian Acad. Sci. Eng., 9, 73–90.

SWAN team, 2008, SWAN Cycle III version 40.72.

Suursaar Ü., Astok V., Alenius P., Kullas T., Otsmann M., 1998, *Thermohaline regime and currents in the Suur Strait and Hari Strait in 1996–1997*, EMI Rep. Ser., 9, 6–22.

Suursaar Ü., Astok V., Kullas T., Nõmm A., Otsmann M., 1995, *Currents in the Suur Strait and their role in the nutrient exchange between the Gulf of Riga and the Baltic Proper*, Proc. Estonian Acad. Sci. Ecol., 5, 103–123.

Suursaar Ü., Astok V., Kullas T., Otsmann M., Alenius P., 1996, *Thermohaline regime and currents in the Suur Strait in 1993–1995*, EMI Rep. Ser., 3, 7–58.

Suursaar Ü., Kullas T., Otsmann M., 2002, *A model study of sea level variations in the Gulf of Riga and the Väinameri Sea*, Cont. Shelf Res., 22 (14), 2001–2019.

Van Rijn L. C., 2007, *Unified view of sediment transport by currents and waves 1: initiation of motion, bed roughness and bed-load transport*, J. Hydraul. Eng.–ASCE, 133 (6), 649–667.

Van der Westhuysen A. J., Zijlema M., Battjes J. A., 2007, *Nonlinear saturation-based whitecapping dissipation in SWAN for deep and shallow water*, Coast. Eng., 54 (2), 151–170.